Phase equilibria and phase transformations in the Ti-rich corner of the Fe–Ni–Ti system

P. Riani, G. Cacciamani, Y. Thebaut and J. Lacaze

Dipartimento di Chimica e Chimica Industriale, Università di Genova, via Dodecaneso 31, I-16146 Genova, Italy
CIRIMAT, UMR CNRS 5085, ENSIACET, F-31077 Toulouse Cedex 4, France

Abstract

While the main features of the Fe–Ni–Ti system are well known at low Ti content, literature review of the Ti-rich corner revealed inconsistencies between experimental reports. This investigation presents new experimental results, defined to remove the uncertainties concerning melting behavior and solid-state phase equilibria of the (Ni,Fe)Ti_2 phase with the adjacent (Fe,Ni)Ti (B2, CsCl-type structure) and β-Ti (A2, W-type) phases. Six samples have been prepared and examined by differential thermal analysis performed in yttria and alumina crucibles, and by scanning electron microscopy in the as-cast state as well as equilibrated at 900 °C.

Keywords: A. Ternary alloy systems; A. Intermetallics, miscellaneous; B. Phase diagrams; D. Microstructure

1. Introduction

Fe–Ni–Ti is an important ternary system relevant to different kinds of materials: from special steels and Ni-based superalloys to alloyed aluminides, from Ti-based corrosion-resistant alloys to shape memory alloys and amorphous materials. Fe–Ni–Ti is also a sub-system of the Al–Fe–Ni–Ti quaternary system, which is the core system of COST 535 “THALU”, a European project aimed at the investigation of the constitutional properties of alloyed aluminides by means of experiments, thermodynamic and ab initio calculations. A review of the ternary Fe–Ni–Ti system provided by Gupta [1] was mainly based on the works by Vogel and Wallbaum [2], Speich [3] and Van Loo et al. [4]. From the first two of these works and the limiting binary systems, Gupta proposed a schematic liquidus projection. It is shown in Fig. 1 according to the revision by Cacciamani et al. [5] in the Ti-rich corner, as discussed and summarized below. The binary invariant points selected to draw this figure agree with the assessments of Lee [6] for the Fe–Ni system, Kumar [7] for the Fe–Ti system and Bellen et al. [8] for the Ni–Ti one. Van Loo et al. [4] provided the 900 °C isothermal section shown in Fig. 2. This figure indicates that every binary compound, $NiTi_2$, (Fe,Ni)Ti, Fe_2Ti and Ni_3Ti, presents significant solubility for the third element and that no stable ternary compound occurs at that temperature. As a matter of fact, no ternary compound was found in this system at any temperature. It is worth mentioning the complete solubility of Fe and Ni in the ordered B2-(Fe,Ni)Ti phase which was previously evidenced by Dudkina and Kornilov [9]. Abramycheva et al. [10] realized a study similar to the one carried out by Van Loo et al. [4] but at 1000 °C from which they drew an isothermal section that is mostly similar to Fig. 2 apart from the presence of a liquid field around point e_5 in Fig. 1 (which is the binary eutectic liquid/β-Ti/NiTi equilibrium at 942 °C).

Fig. 1. Liquidus projection of the Fe–Ni–Ti system according to Cacciamani et al. [5].

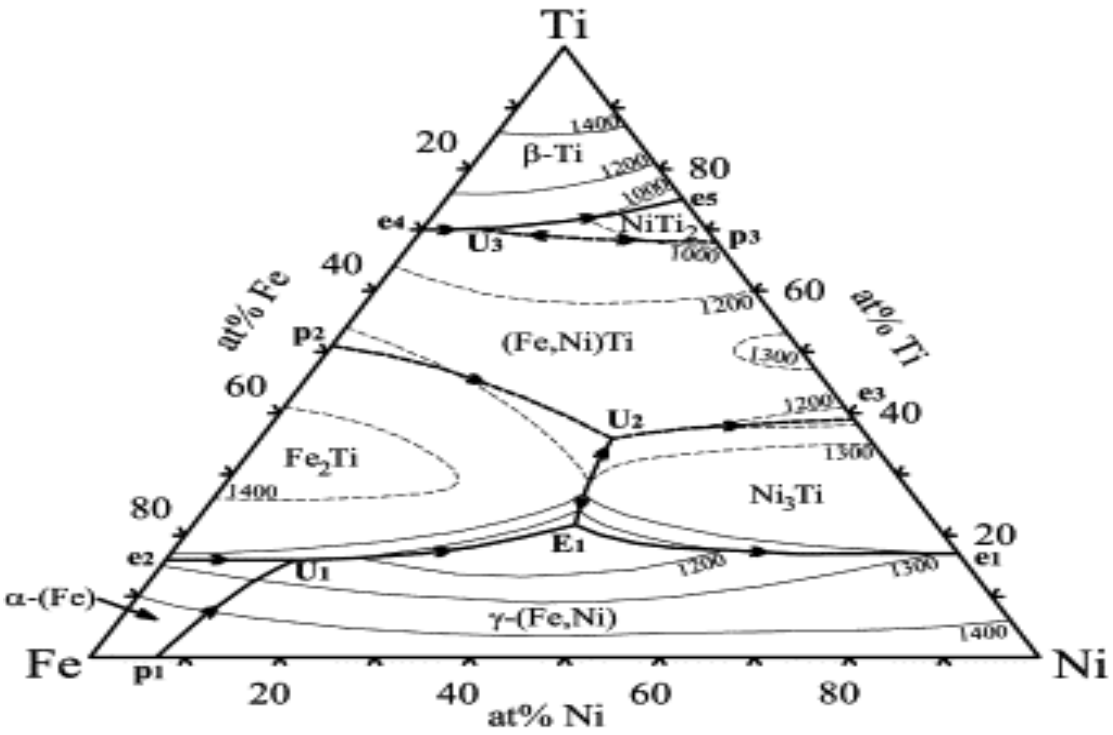

Fig. 2. Fe–Ni–Ti isothermal section at 900 °C after Van Loo et al. [4]. Solid circles represent phase compositions according to the accepted assessments of the binary systems. Empty circles are experimental data read from the provided figure [4]: they are linked with tie-lines drawn with dots. Three-phase triangles shown with interrupted lines as well as single-phase fields were guessed by Van Loo et al.[4].

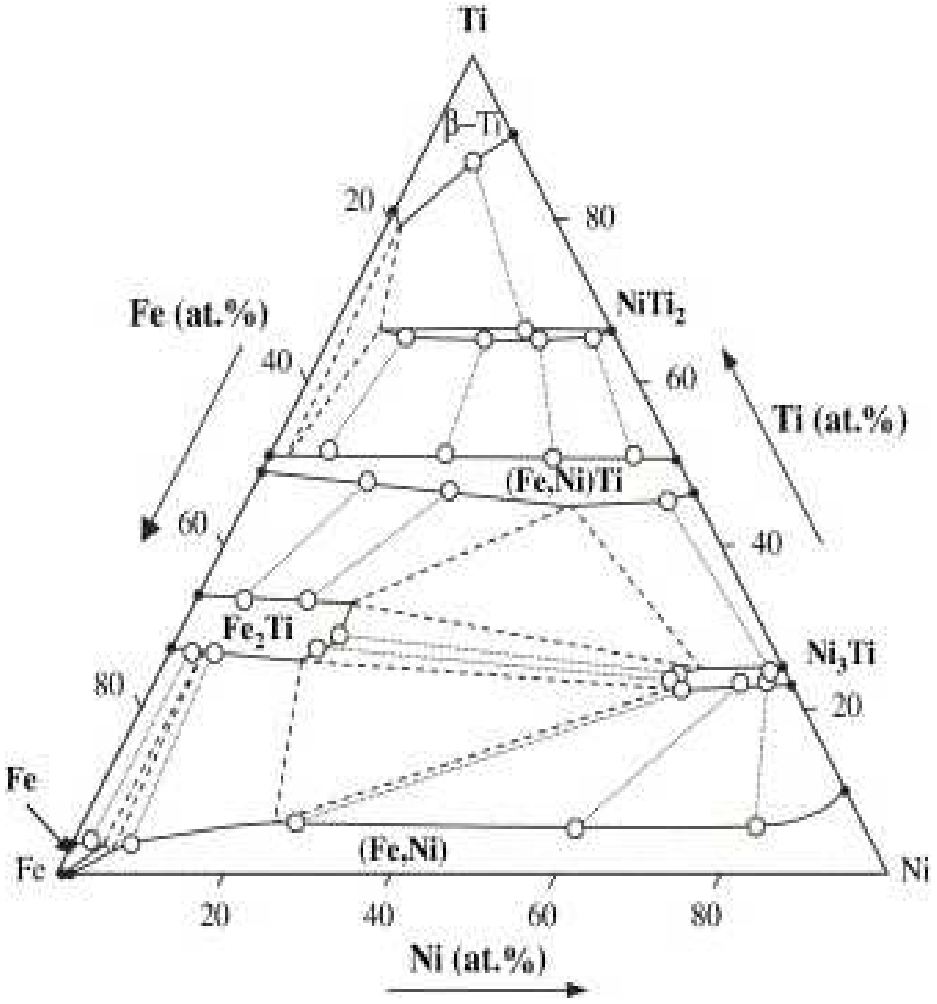

In a re-assessment of his previous review, Gupta [11] accounted for the work of Alisova et al. [12] who provided three vertical sections of the diagram in the Ti-rich region. These sections were selected with Fe:Ni equal to 3:1, 1:1 and 1:3, respectively, and suggested that the peritectic reaction giving $NiTi_2$ occurs only in the section at Fe:Ni = 1:3 closest to the Ni–Ti side. Accordingly, Gupta [11] located the four-phase equilibrium between liquid, β-Ti, $NiTi_2$ and B2-(Fe,Ni)Ti at a very low Fe content. The vertical sections determined by Alisova et al.

[12] are, however, in contradiction with the isothermal sections by Van Loo et al. [4] and by Abramycheva et al. [10], as effectively noticed by these latter authors and discussed by Cacciamani et al. [5]. Finally, Efimenko et al. [13] observed experimentally that $NiTi_2$ precipitates from melts with much higher Fe contents than suggested by Abramycheva et al. [10]. In order to remove this discrepancy, the present work was undertaken on a series of alloys at 66 at.% of Ti and involved structural analysis of homogenized samples and as-cast materials as well as differential thermal analysis of the first ones.

2. Experimental details

Several alloys with composition along the $FeTi_2$–$NiTi_2$ line were prepared by arc melting small pieces of the pure elements (99.99 wt% Fe, 99.99 wt% Ni, and 99.98 wt% Ti) in an argon atmosphere. The alloys were then sealed in quartz ampoules filled with argon, heat treated for 15 days at 900 °C to reach equilibrium and then quenched in water. The samples were observed by optical (Leica DM 4000M) and scanning electron microscopies (SEM, Cambridge Stereoscan 200) and analysed by energy dispersive spectroscopy (EDS, Oxford INCA Energy 300) to evaluate the composition of the coexisting phases and of the overall samples. The microstructure of the alloys was investigated after surface polishing by using SiC papers and diamond paste down to 1/4 μm particle size. SEM imaging in backscattered electron mode as well as EDS analyses were performed on unetched samples. Quantitative EDS analyses were carried out using an acceleration voltage of 20 kV and a counting time of 50 s using a cobalt standard in order to monitor beam current, gain and resolution of the spectrometer. Apparent compositions were finally corrected for ZAF (atomic number, absorption and fluorescence) effects using pure elements as standards. The standard deviation for each element was estimated at ±0.5 at.% for phase analysis and at ±1.0 at.% for global analysis.

Small part of the samples was then cut out for differential thermal analysis (DTA, SETARAM SETSYS) and the remaining part was re-melted and solidified by natural cooling in the arc furnace for observation of the as-cast microstructure. The composition of the phases in the as-cast state was also evaluated by means of EDS (PGT analyzer) on an LEO scanning electron microscope, under experimental conditions very similar to those listed above except that the counting time was 100 s. According to the PGT software, the standard deviation in this case was about 0.5 at% for Ni and 0.8 at% for Fe and Ti.

DTA experiments were first performed in yttria crucibles (provided by MaTeck GmbH, Jülich, Germany) with the hope to avoid extensive reaction between the alloy and the crucible. Before each experiment, the DTA cell was twice evacuated and filled with high purity argon. Runs were performed at a scanning rate of 15 K/min under a continuous flux of argon. No exothermic reaction was observed after melting, as it is the case when alumina crucibles are used. However, it was noted that the sample stuck to the wall of the crucible, thus showing some limited reaction with it. Moreover, WDS analysis (CAMECA SX-50 microprobe) of a sample which could be separated from the crucible showed extensive pollution with oxygen. It was thus decided to consider only the data for start of melting of the alloys and it was checked that similar data could be obtained with standard alumina crucibles. All the DTA records were thus carried out twice. Before and after the whole series of recording, the DTA cell was calibrated using melting temperature T_m of pure Ag as illustrated with the runs at 5 and 15 K/min shown in Fig. 3. As expected, an increased scanning rate shifts more and more the melting signal with respect to the tabulated temperature.

Fig. 3. DTA records obtained on heating pure Ag at various scanning rates. The tabulated melting temperature T_m of Ag is indicated.

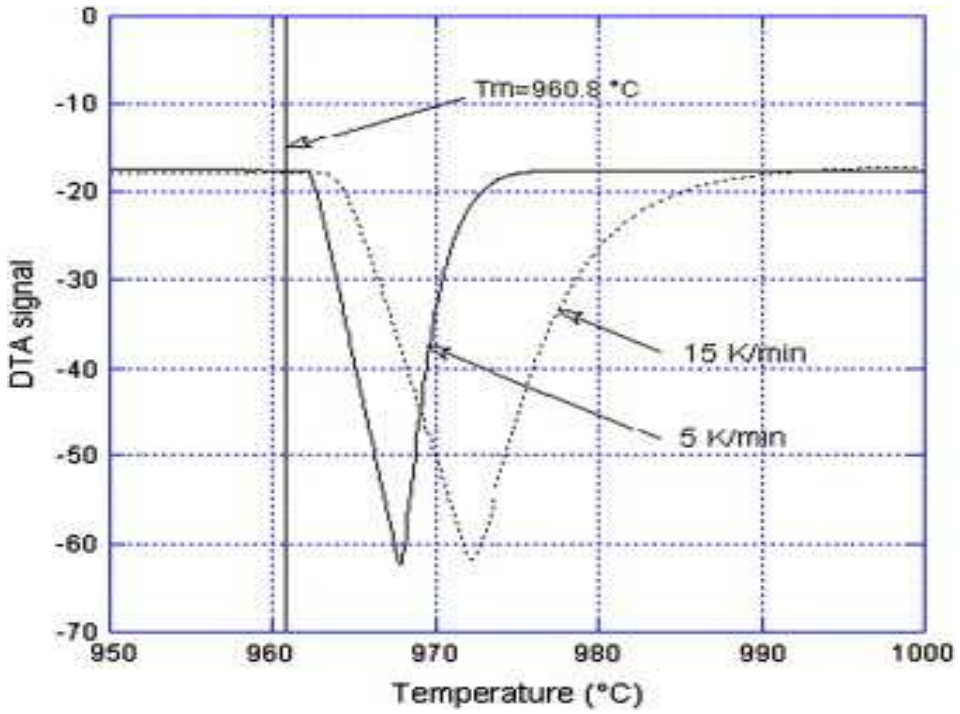

3. Results

3.1. Homogenized alloys

The list of the samples prepared and the results of the phase analysis are reported in Table 1. Except for alloy A which contained three phases, all other homogenized alloys showed a two-phase microstructure. The minor phase, denoted as phase 1 in Table 1, has a lower Ti content than phase 2 and presents remaining outlines of dendritic solidification in all samples, as illustrated in Fig. 4 for sample C. In alloy A, a third phase shows up with even higher Ti content than phase 2. On the basis of Fig. 2, it was easy to establish that phase 1 corresponds to B2-(Fe,Ni)Ti, phase 2 to (Fe,Ni)Ti_2 and phase 3 to the A2 β-Ti solid solution. The dendritic shape adopted by phase 1 shows that it is the primary phase formed upon solidification for all six alloys investigated. Except for alloy A, (Fe,Ni)Ti_2 forms incongruently from liquid and B2-(Fe,Ni)Ti, as it is also the case in the binary Ni–Ti system. In the case of alloy A, the three-phase microstructure observed after homogenization could not be interpreted so straightforwardly.

Table 1.

Compositions and phase analyses of the homogenized (Homog.) and as-cast alloys determined by EDS

Sample	**Sample composition Fe/Ni/Ti (at.%)**	**Sample state**	**First phase: B2-(Fe,Ni)Ti Fe/Ni/Ti (at.%)**	**Second phase: (Fe,Ni)Ti_2 Fe/Ni/Ti (at.%)**	**Third phase: A2 β-Ti Fe/Ni/Ti (at.%)**	**Fourth phase: Fe/Ni/Ti (at.%)**
A	29.0/4.0/67.0	Homog.	44.0/4.0/52.0	26.0/6.5/67.5	18.0/1.5/80.5	
		As-cast	43.5/3.8/52.7	22.5/6.5/71.0	20.2/1.9/77.9	33.3/4.3/62.4
B	25.0/8.0/67.0	Homog.	41.5/6.5/52.0	23.5/9.5/67.0		
		As-cast	37.5/10.2/52.3	22.6/9.9/67.5	17.4/3.6/79.0	
C	20.0/13.5/66.5	Homog.	35.0/13.0/52.0	19.0/13.5/67.5		
		As-cast	30.4/16.6/53.0	18.8/13.8/67.4	12.7/5.3/82.0	

Sample	Sample composition Fe/Ni/Ti (at.%)	Sample state	First phase: B2-(Fe,Ni)Ti Fe/Ni/Ti (at.%)	Second phase: (Fe,Ni)Ti_2 Fe/Ni/Ti (at.%)	Third phase: A2 β-Ti Fe/Ni/Ti (at.%)	Fourth phase: Fe/Ni/Ti (at.%)
D	14.5/19.0/66.5	Homog.	25.0/23.0/52.0	14.0/18.5/67.5		
		As-cast	23.4/24.2/52.4	14.8/17.9/67.3	7.9/8.9/83.2	
E	10.0/24.0/66.0	Homog.	16.5/31.5/52.0	9.5/23.5/67.0		
		As-cast	16.0/31.4/52.6	8.2/24.1/67.7	4.6/17.6/77.8	
F	5.0/28.5/66.5	Homog.	7.5/41.0/51.5	4.5/28.0/67.5		
		As-cast	6.7/41.2/52.1	5.0/27.8/67.2		

Fig. 4. Backscattered electron image of the microstructure of alloy C after homogenization at 900 °C. The brighter phase, lower in Ti, shows typical dendritic outline and is associated with B2-(Fe,Ni)Ti while the darker one is (Fe,Ni)Ti_2.

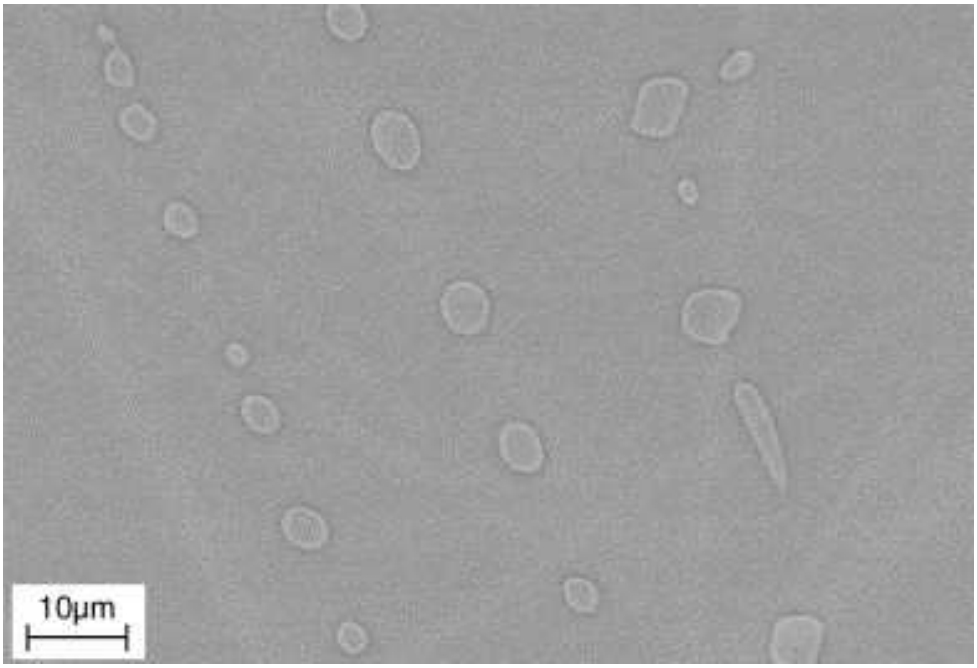

In Fig. 5 the overall compositions of the alloys (solid circles) and those of the individual phases (solid squares) are plotted. Solid diamonds on the sides represent the composition of the binary phases at 900 °C according to the accepted binary phase diagrams (see Ref. [5]). Tie-lines for the two-phase samples and tie-triangle for sample A are also drawn. These equilibria are very similar to those determined by Van Loo et al. [4] and reproduced in Fig. 2, consisting in a three-phase equilibrium β-Ti/(Fe,Ni)Ti_2/B2 close to the Fe–Ti side and an extended (Fe,Ni)Ti_2/B2 two-phase field towards the Ni–Ti side.

Fig. 5. Composition of the alloys (solid circles) and of the individual phases after homogenization (solid squares) and in the as-cast state (open symbols). Binary data corresponding to the phases' composition at 900 °C have been plotted with solid diamonds.

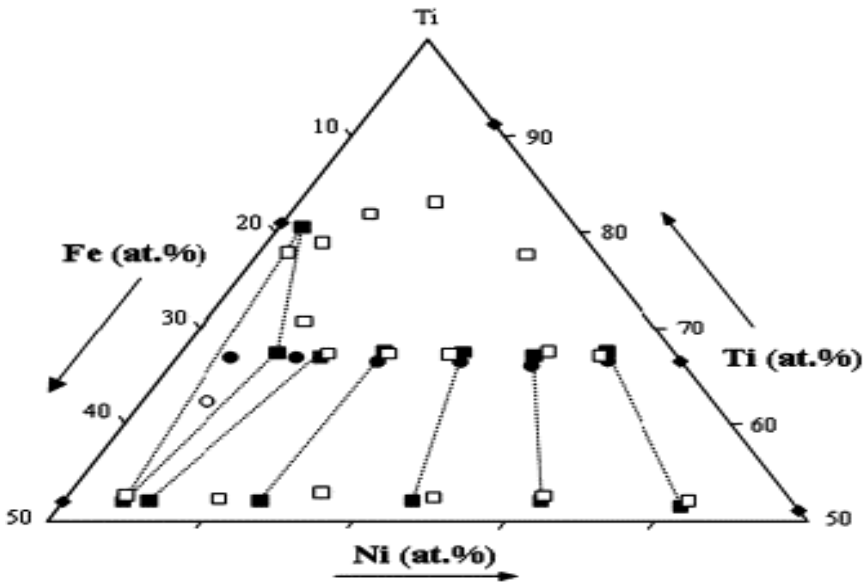

DTA peaks recorded on heating of homogenized alloys A–F are illustrated in Fig. 6. Owing to the smooth shape of the peaks, the solidus temperature was estimated at the intersection of the extrapolated base line with the back-extrapolated peak rise shown with interrupted lines in the figure. According to the Ag calibration in Fig. 3, the evaluated temperatures were decreased by 3 °C. Fig. 7 shows the experimental solidus temperatures as a function of the iron content of the alloy. The reproducibility of the records was excellent, with the highest difference in the evaluation of the solidus temperature amounting to a few degrees in the case of alloy D (15 at.% of Fe). For this alloy, the two dots representing the solidus temperature can be distinguished in Fig. 7, in all other cases they cannot. In the same figure, assessed

temperatures of the binary reactions have been added and they show that the present set of results is highly consistent with them. The evolution of the solidus temperature suggests a maximum at about 1030 °C and 15–20 at% Fe and a minimum at about 1025 °C and 25 at% Fe. The minimum could be associated with the invariant equilibrium between liquid, β-Ti, $NiTi_2$ and B2-(Fe,Ni)Ti which should thus be quite close to the Ti–Fe side.

Fig. 6. DTA records for alloys A–F obtained on heating at 15 K/min. The curves were shifted arbitrarily along the ordinate axis for better clarity. The solidus temperatures have been estimated by extrapolation as shown in the figure with interrupted lines. Before plotting on Fig. 7, the values here indicated diminished by 3 °C to account for heating rate effect (see text).

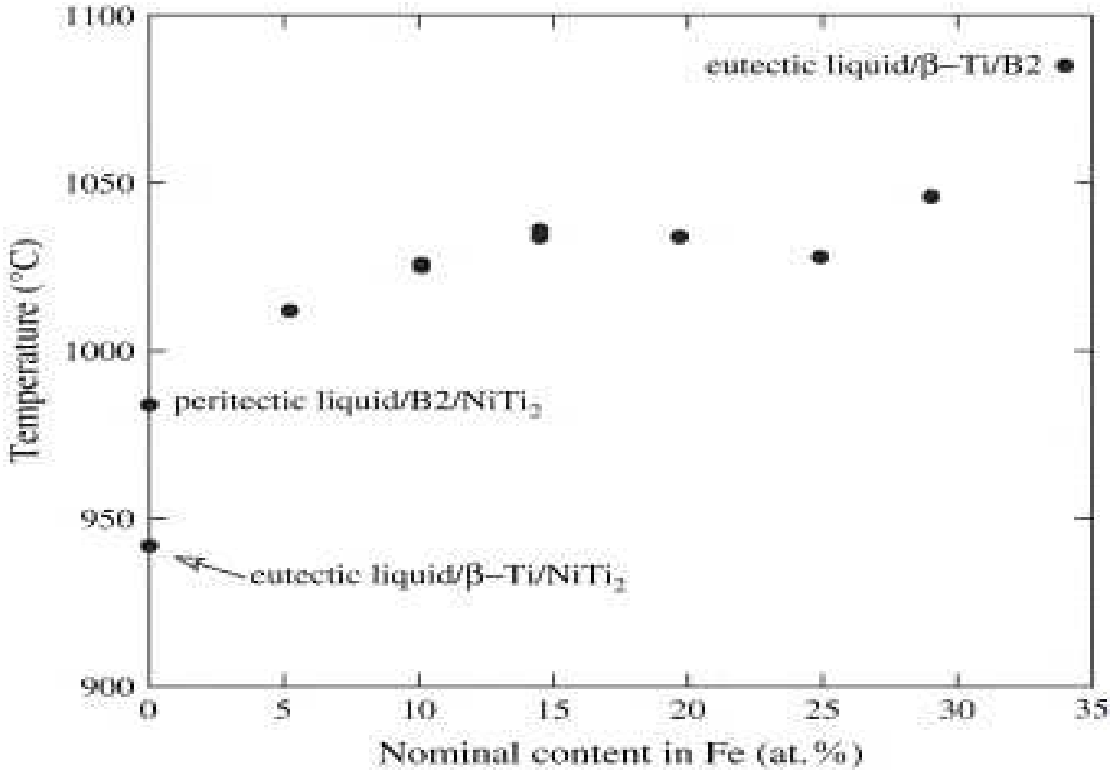

Fig. 7. Solidus temperature of the homogenized alloys as a function of iron content.

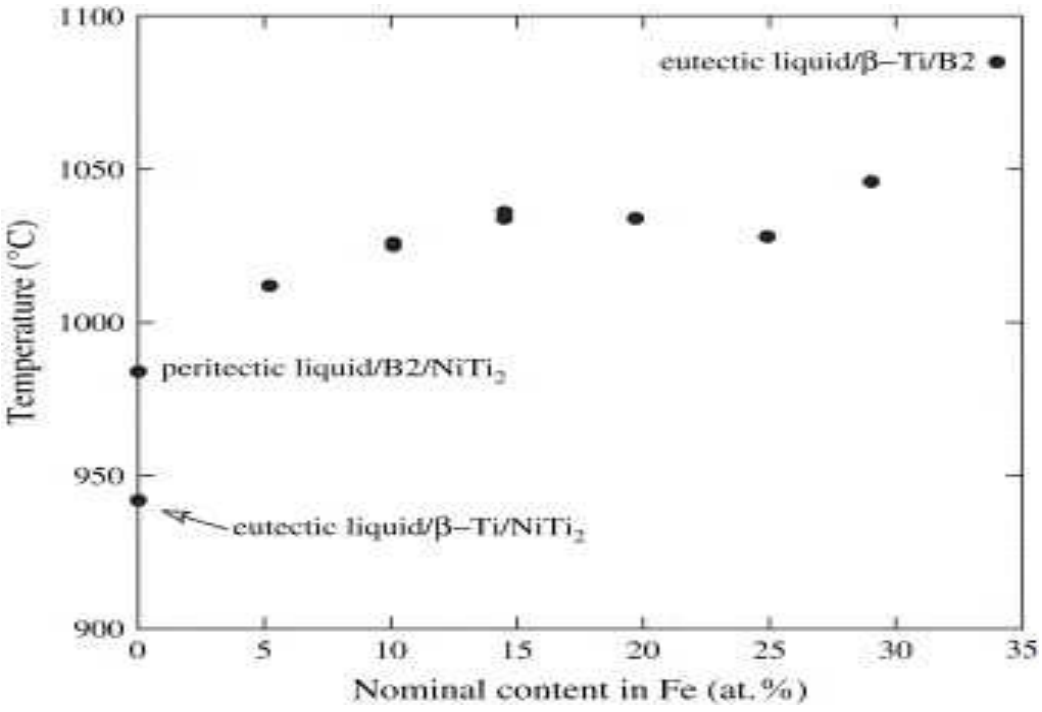

3.2. As-cast samples

The microstructures of the as-cast samples show different aspects when compared to the equilibrated alloys. Alloy A apparently presents four phases (Fig. 8(a)), alloys B–E show three phases (Fig. 8(b)), and alloy F shows only two phases. In Table 1, the phases have been sorted according to their Ti content, except for the fourth phase in sample A. It can be seen that the data for phases 1–3 in Fig. 5 (empty squares), are very close to the data obtained on homogenized samples for phase 1 corresponding to B2-(Fe,Ni)Ti and phase 2 corresponding to (Fe,Ni)Ti_2. The measurements on phase 3 (β-Ti) are well located between the two extreme values on the binary sides apart from the one obtained from alloy E which appears at too high Fe level. As expected, it is seen that, for alloy A, the Ni content of β-Ti is slightly lower in the sample homogenized at 900 °C than in the as-cast alloy because the solubility of Ti in this phase decreases with temperature.

Fig. 8. Microstructure of as-cast samples of alloys A (a) and C (b). Dark grey is β-Ti, intermediate grey is (Fe,Ni)Ti_2, and light grey is B2-(Fe,Ni)Ti. The white precipitates in figure (a) are also associated with this latter phase (see text).

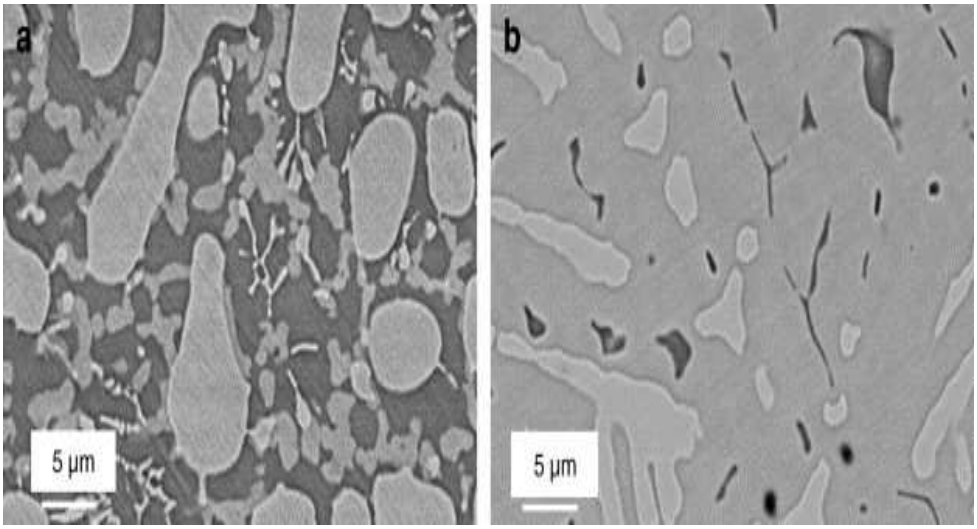

As for the homogenized samples, the B2 phase appears in every case as a dendritic primary phase. Moreover, in alloys B–F there are clear indications that B2 partly dissolved because of a peritectic reaction giving (Fe,Ni)Ti_2. Other features observed are that (Fe,Ni)Ti_2 grows also dendritically around the primary B2 phase and that β-Ti deposits as a separate phase (divorced eutectic) in the last solidifying interdendritic areas (Fig. 8(b)).

In the case of alloy A, primary dendrites are surrounded mainly by β-Ti (Fig. 8(a)) which appears to be the second phase formed during solidification. (Fe,Ni)Ti_2 forms rather irregularly shaped deposits with a smaller size than β-Ti. Finally, thin and elongated precipitates of a phase with bright contrast are seen within β-Ti. The composition of this fourth phase has been reported with an empty circle in Fig. 5. It is seen that it lies in between the compositions of (Fe,Ni)Ti_2 and B2 phases, so that the value estimated represents certainly an average of the compositions of these two phases because of its small size. The shape, size and contrast of this phase suggest that it is the B2-(Fe,Ni)Ti that formed by solid-state precipitation during cooling.

4. Conclusions

Present results show that the $NiTi_2$ phase is stabilized by substitution of Fe for Ni, as suggested by the increase in the solidus temperature with the Fe content (see Fig. 9). Nevertheless, $NiTi_2$ cannot overtake the B2 phase which was observed to be the primary phase upon solidification in the whole composition range investigated. This allows to draw the tentative $FeTi_2$–$NiTi_2$ section of the phase diagram shown in Fig. 9, according to which the invariant point between liquid, β-Ti, $NiTi_2$ and B2-(Fe,Ni)Ti is much closer to the Fe–Ti

side than previously suggested [11] and should be of the U-type: liquid + (Fe,Ni)Ti ↔ β-Ti + $(Fe,Ni)Ti_2$.

Fig. 9. Tentative vertical section of the Fe–Ni–Ti phase diagram at x_{Ti} = 0.66. The points are the data plotted in Fig. 7.

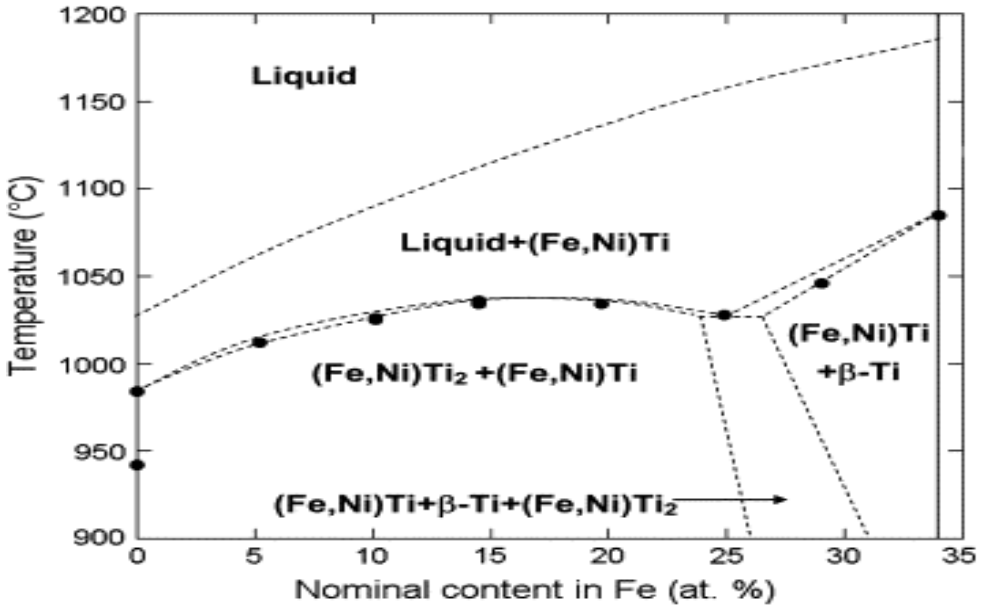

Acknowledgements

This work was performed within the frame of the COST ACTION 535 (THALU) and the partial support of COST-ESF and Italian project MIUR-PRIN2003091235 is acknowledged. The WDS analyses have been carried out in the “Service d'analyse de l'Université P. Sabatier”, Toulouse, France.

References

K.P. Gupta, Phase diagrams of ternary nickel alloys, part 1, Indian Institute of Metals (1990) p. 321–43.

R. Vogel and H.S. Wallbaum, *Arch Eisenhuttenwesen* **12** (1938), pp. 299–304.

G.R. Speich, *Trans Met Soc AIME* **227** (1963), pp. 754–762.

F.J.J. Van Loo, J.V.G.A. Vrolifk and G.F. Bastin, *J Less Common Met* **77** (1981), pp. 121–130.

G. Cacciamani, J. De Keyzer, R. Ferro, U. Klotz, J. Lacaze and P. Wollants, Intermetallics, doi:10.1016/intermet.2005.11.028 (2006).

B.J. Lee, *Calphad* **17** (1993), pp. 251–268.

Hari Kumar KC. XXVIII CALPHAD meeting. Grenoble; 1999.

P. Bellen, K.C. Hari Kumar and P. Wollants, *Z Metallkd* **87** (1996), pp. 972–978.

L.P. Dudkina and I.I. Kornilov, *Russ Metall* **4** (1967), pp. 98–101.

N.L. Abramycheva, I.V. V'yunitskii, K.B. Kalmykov and S.F. Dunaev, *Vestn Mosk Univ Ser 2 Khim* **40** (1999), pp. 139–143.

K.P. Gupta, *J Phase Equilib* **22** (2001), pp. 171–175.

S.P. Alisova, P.B. Budberg, T.I. Barmina and N.V. Lutskaya, *Russ Metall* **1** (1994), pp. 117–121.

L.P. Efimenko, L.P. Petrova and S.I. Sviridov, *Russ Metall* **3** (2000), pp. 42–46.

Corresponding author. Tel.: +39 010 353 6152; fax: +39 010 362 5051.

Original text : Elsevier.com